Numerical Simulations of Instabilities in Single-Hole Orifice Elements

Vineet Ahuja[1] and Ashvin Hosangadi[2]
Combustion Research and Flow Technology, Inc., Pipersville, PA, 18947

Matthew A. Hitt[3] and David M. Lineberry[4]
University of Alabama in Huntsville, Huntsville, AL, 35899

An orifice element is commonly used in liquid rocket engine test facilities either as a flow metering device, a damper for acoustic resonance or to provide a large reduction in pressure over a very small distance in the piping system. While the orifice as a device is largely effective in stepping down pressure, it is also susceptible to a wake-vortex type instability that generates pressure fluctuations that propagate downstream and interact with other elements of the test facility resulting in structural vibrations. Furthermore in piping systems an unstable feedback loop can exist between the vortex shedding and acoustic perturbations from upstream components resulting in an amplification of the modes convecting downstream. Such was the case in several tests conducted at NASA as well as in the Ariane 5 strap-on P230 engine in a static firing test where pressure oscillations of 0.5% resulted in 5% thrust oscillations. Exacerbating the situation in cryogenic test facilities, is the possibility of the formation of vapor clouds when the pressure in the wake falls below the vapor pressure leading to a cavitation instability that has a lower frequency than the primary wake-vortex instability. The cavitation instability has the potential for high amplitude fluctuations that can cause catastrophic damage in the facility. In this paper high-fidelity multi-phase numerical simulations of an orifice element are used to characterize the different instabilities, understand the dominant instability mechanisms and identify the tonal content of the instabilities.

I. Introduction

ORIFICES and venturis are versatile devices that find widespread application in aerospace propulsion systems, test facilities, expansive piping systems, pressurized water reactors and reciprocating compressor systems. Although simplistic in their structural design, their versatility stems from their functionality: for example, due to the presence of a vena contracta, orifices and venturis are commonly used as flow metering devices in piping systems and test facilities; the presence of two-phase flow through an orifice helps it in serving as an atomizer in liquid rocket injector elements; given its capacity for mode conversion, an orifice can also serve as a dynamical phase converter as part of a control system that inhibits combustion instabilities; orifice plates are also commonly used in various aerospace applications such as segmented solid propellant rocket motors as inhibitors of acoustic fluctuations in those systems. However, the most common application of an orifice is one of providing resistance in helping to step down pressure in a piping system. This is particularly important for high pressure systems such as seen in liquid rocket engine test facilities and pressurized water reactors, where a finite length of pipe is available to step the pressure down.

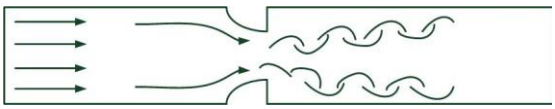

Figure 1. Vortex Shedding Instability through Single-Hole Orifice

The performance of an orifice is usually characterized by the average discharge coefficient which is represented

[1]Senior Research Scientist, CRAFT Tech, Inc., 6210 Keller's Church Road, AIAA Senior Member
[2]Principal Scientist, CRAFT Tech, Inc., 6210 Keller's Church Road, AIAA Senior Member
[3]Graduate Research Assistant, UAHuntsville Propulsion Research Center, TH S225, AIAA Student Member
[4]Research Engineer, UAHuntsville Propulsion Research Center, TH S225, AIAA Senior Member

as the ratio of the measured and theoretical flow rates and engineers and designers size the orifice plates in a system based on the Reynolds Number of the flow, mass flow rates and the required pressure drop. The pressure drop through the orifice results from a combination of flow acceleration, flow resistance due to frictional losses and flow turning. However, as the flow negotiates the turn in the orifice and flows downstream a hydrodynamic instability results leading to vortex shedding from the lip/edge of the orifice (Figure 1). The vortex shedding is primarily responsible for the acoustic whistling which has been observed [1] and is similar to the case of shedding from cylinders in cross-flows as well as the flow separation associated with cavities. The pressure fluctuations associated with the shedding process can result in the formation of cavitation bubbles/clouds whenever the pressure fluctuations are large enough such that the pressure locally falls below the saturation pressure [2]. This is shown in Figure 2 where a vapor wake is formed behind the lip of the orifice; as the vapor trail encounters a low pressure region large vapor clouds are formed that migrate downstream. In such cases, the cavitation related instability is a sub-harmonic of the wake-vortex instability or a lower frequency instability than the wake vortex instability. In certain cases the energy may be spread across multiple lower frequency modes. On the other hand, in regimes of high mass flow rates, when the venturi or orifice operates in a "choked flow" condition the pressure drop in the vena contracta is large enough resulting in large vapor cavities [3]. Flow transients in the piping system can disrupt these cavities causing the shedding and convection of vapor clouds in the downstream section of the piping system. Furthermore, in cryogenic fluids, local temperature gradients can cause condensation of these clouds leading to violent high amplitude pressure spikes that can cause catastrophic damage [4].

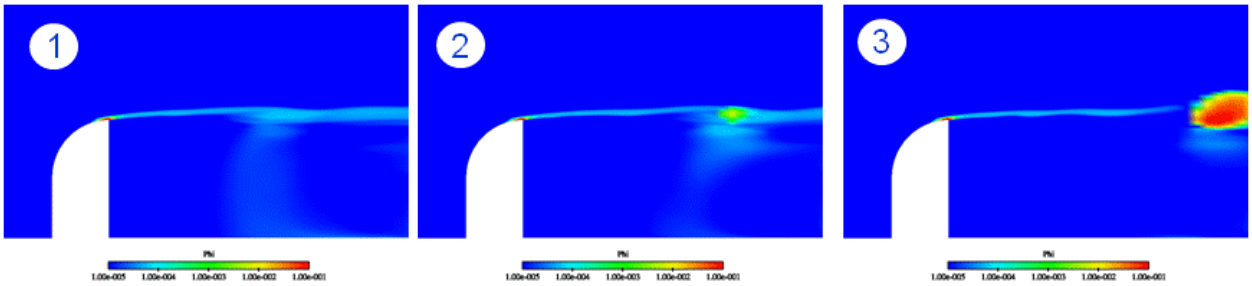

Figure 2. Development of Vapor Clouds close to the lip of the orifice

Since the orifice element is usually a part of a larger piping system that includes valves, pumps, turning ducts, diffusers etc., the orifice rarely operates under nominally "steady" conditions and is usually subject to pressure and/or velocity fluctuations. Even in non-cavitating regimes, small scale perturbations in the upstream piping elicit a highly complex non-linear dynamic response from the orifice resulting in large scale fluctuations that are convected downstream. In a study by Noiray et al. [5], it is postulated that a mode conversion takes place in acoustically modulated confined jets through an orifice. The authors in this study excited a flow through an orifice with a loudspeaker. The acoustic velocity at the orifice constriction is reduced and compensated by the generation of convective perturbations that result in vortices downstream of the orifice, thereby showing a conversion of acoustic oscillations to convective modes. Another study was carried out at Purdue University (MacDonald et al. [6]) where the impact of a downstream pressure oscillation (such as in a combustor chamber) on the flow through plain orifice injector was studied. The study concluded that the overall response of the orifice injector was bounded by the response predicted by the one-dimensional linearized theory. The exception to this was a local resonance condition when the driving frequency was close to the natural frequency of the Kelvin Helmholtz instability in the orifice. More importantly it needs to be emphasized that instability modes whether initiated in the orifice section or amplified therein can have a profound effect on the operation of components downstream of the orifice. Such events significantly increase the associated risk with operating the facility and result in shutting down the testing loop and re-design of the loop configuration. Moreover, large pressure fluctuations related to instabilities in orifice elements have also been observed in feed systems on NASA SSC test facilities such as E-1/A-2 test stands as well as in the Ariane 5 strap-on P230 engine in a static firing test.

Computational simulations can play an integral role in supporting testing and developmental activities by identifying and characterizing these instabilities. However, the diversity of flow regimes and instability mechanisms place very stringent requirements on any computational framework that could be used for such analyses. For example, the identification of dominant frequencies associated with flow instabilities through an orifice requires high order numerics, and advanced turbulence modeling capabilities to resolve the rich spectrum of spatial and temporal scales, coupled with embedded models for unsteady cavitation that capture the two-phase flow dynamics. Furthermore liquid rocket facilities and systems operate with cryogenic fluids where the operating point is in close proximity to the critical temperature, leading to substantial thermal effects and property variations associated with

such flows. Our cavitation models account for the coupling of thermodynamic processes with the cavitation processes and have accurately captured such effects as leading edge pressure and temperature depression due to evaporative cooling, and frothy cavitation zones that are the hallmark of cavitated regions in cryogenic fluids. Furthermore, with the incorporation of an unsteady cavitation model we are able to predict amplitudes and frequencies of dynamic pressure loads and track dense bubble clouds that shear predominantly vaporous regions such as cavities and vortex cores. *In this paper, we utilize our high-fidelity multi-phase model [2, 4] to characterize the instabilities in cryogenic flow through an orifice in a pipe system. The simulations provide insight into the physics governing both the wake-vortex instability and the cavitation instability. The simulations were also able to pick up tones associated with the interaction of the jet with the wall.*

II. Methodology

A. Multi-phase Equation System

We give a very brief overview of the basic multiphase equation system here and refer the reader to Hosangadi and Ahuja [4] for more details. The equation system is written solved in a pressure based form as:

$$\Gamma \frac{\partial Q_v}{\partial t} + \frac{\partial E}{\partial x} + \frac{\partial F}{\partial y} + \frac{\partial G}{\partial z} = \mathrm{S} + \mathrm{D_v} \tag{1}$$

$$Q_v = \begin{pmatrix} P \\ u \\ v \\ w \\ \phi_g \\ h_m \\ k \\ \varepsilon \end{pmatrix} \quad E = \begin{pmatrix} \rho_m u \\ \rho_m u^2 + P \\ \rho_m uv \\ \rho_m uw \\ \rho_g \phi_g u \\ \rho_m h_m u \\ \rho_m ku \\ \rho_m \varepsilon u \end{pmatrix} \quad S = \begin{pmatrix} 0 \\ 0 \\ 0 \\ 0 \\ m_t \\ m_t h_{fg} \\ S_k \\ S_\varepsilon \end{pmatrix} \tag{2}$$

The vectors Qv, E and S are given above. The matrix $\Gamma (= \partial Q / \partial Q_v)$ defines the transformation from the conservative to primitive variables and may further be preconditioned to obtain an efficient time-marching scheme.

The source term for the vapor phase arises due to cavitation where m_t is the net rate of vapor mass generation (or condensation), and the corresponding source term for the energy equation is given as $m_t h_{fg}$ where h_{fg} is the change in enthalpy resulting from the phase change and is a function of the local fluid temperature. These phase change source terms are discussed in a later section.

The mixture density, enthalpy, and vapor porosity are related by the following relations locally in a given cell volume:

$$\rho_m = \rho_g \phi_g + \rho_L \phi_L \tag{3}$$

$$\rho_m h_m = \rho_g \phi_g h_g + \rho_L \phi_L h_L \tag{4}$$

$$1 = \phi_g + \phi_L \tag{5}$$

where ρg , ρL are the physical material densities, while h_g and h_L are the sensible enthalpy of the vapor and liquid phase respectively, and in general are functions of both the local temperature and pressure. In our study here, these properties were generated from the Standard thermodynamic database 12 available from NIST for pure fluids [7]. The thermodynamic properties of the fluid where specified using the saturation values from the table corresponding to the local temperature of the fluid. Equations (1)-(2) represent a stiff system with large variations in the acoustic speed that are a function of the local multi-phase composition. Preconditioning techniques are used to overcome this stiffness and obtain an efficient numerical scheme [4].

B. Unsteady cavitation model using cloud surface area equation

The new, unsteady cavitation model developed incorporates formulations for bubble dynamics (e.g. Rayleigh-Plesset equation) as an integral part of dense cloud cavitation. By drawing on our experience in dense spray combustion [8], we track the surface area associated with the cavitation cloud as it evolves spatially and temporally. We note that this Eulerian procedure has been formulated within the premise of a dense bubble cloud where a large number of bubbles are present. Bubbles comprising the cloud will be characterized by their Sauter mean radius, which preserves the ratio of the surface area and volume for the bubbly cloud. Thus, the source term for cavitation will have two independent factors controlling it: a) the net surface area given by the bubble Sauter mean radius, and b) the rate of change of the radius, which may be specified using the Rayleigh-Plesset equation.

The additional equation (shown in 1-D form for discussion purposes) for the bubble surface area is given as:

$$\frac{\partial S_g}{\partial t} + \frac{\partial S_g u}{\partial x} = s_t \tag{6}$$

Here s_t is the source terms to the cloud surface area equation derived in a manner consistent with the Rayleigh Plesset equation and is defined later. For clarity, we repeat the vapor mass conservation, which was already included as part of the original multi-phase system (Eqn. (2)),

$$\frac{\partial \rho_g \phi_g}{\partial t} + \frac{\partial \rho_g \phi_g u}{\partial x} = m_t \tag{7}$$

The dependent variables S_g and ϕ_g may be written as

$$S_g = N*4.0*\pi*r^2, \quad \phi_g = N*4.0*\pi*r^3/3.0 \tag{8}$$

where N is the number density of bubbles, and r the Sauter mean radius of bubbles at each grid point. Thus, the Sauter mean radius, r, that conserves cloud surface area and volume is defined as, $r = 3*\phi_g / S_g$. Note that no restriction is placed on the vapor volume fraction being dilute. Furthermore we do not restrict the number density of bubbles to be a constant in each cell, and allow them to convect as governed by the hydrodynamics.
The source terms for the net vapor mass transfer and surface area change are given by

$$\begin{aligned} m_t &= \rho_g S_g r_t \\ s_t &= 2.0*S_g r_t / r \end{aligned} \tag{9}$$

where r_t is the rate of change of the radius. To specify the rate of change of radius r_t, the Rayleigh-Plesset Equation could be specified as follows:

$$r\frac{d^2 r}{dt^2} + \frac{3}{2}\left(\frac{dr}{dt}\right)^2 = \frac{1}{\rho_l}\left\{(P_i - P_\infty) - \frac{2\sigma}{r} - \left(\frac{4\mu}{r}\right)\frac{dr}{dt}\right\} \tag{10}$$

However this would require the solution of an additional transport equation for the solution of (dr/dt). In our study a simplified and approximate form for the radius change is used:

$$\frac{dr}{dt} = \pm\left(\frac{2}{3}\right)^{1/2}\left(\frac{abs(P_v - P)}{\rho_l}\right)^{1/2} \tag{11}$$

where the sign of the radius change term depends on whether the bubble is growing or decaying and is dictated by the sign of the $P_v - P$ term. Here, P_v is the vapor pressure, while P is the instantaneous pressure at the grid node point at which the cavitation source term is being computed, and ρ_l is the liquid density. We again emphasize that Eqn. (11) provides the phase change for an individual bubble only while the net mass transfer is given by Eqn. (9) by accounting for the total surface area of bubbles present at a given spatial grid location. Hence a more fundamental unsteady cavitation formulation is derived.

III. Results

A. Single Phase Simulations of Single Hole Orifice Element

Three-dimensional hybrid RANS-LES [9] simulations have been carried out for a pipe with an inner diameter of 0.8 inches with a traditional single-hole orifice with a vena contracta of 0.4 inches. The orifice is not a sharp edge type orifice but rather has a rounded shape to guide the flow smoothly into the vena contracta. This orifice is a sub-scale version of the one utilized at NASA SSC for the 4-inch LOX line. The upstream pipe is long enough to ensure that the flow is well-developed before it encounters the orifice. The operating fluid for this simulation is nitrogen since this will be the fluid of choice to the sub-scale testing. The nominal temperature for this test is 88.75 K. The mass flow rate through the pipe as determined by the sub-scale testing considerations is 3 lbm/s which corresponds to a freestream velocity of 5.58 m/s. The Reynolds Number for the simulation is 400,000 based on the orifice diameter and the inlet pressure was determined to be 94 psi based on a specified back pressure of 80 psi at the exit.

The time averaged pressure distribution is shown in Figure 3 below along with a line plot for the pressure along the axis of the duct and orifice. The pressure drops approximately 24 psi in the throat of the orifice along the centerline and recovers downstream to 80 psi which was the imposed back pressure for the simulation. However, there is a significantly larger drop in pressure along the lip of the orifice near the throat (see Figure 3(a)) than is seen on the centerline plot in Figure 3(b).The vapor pressure for liquid nitrogen at 88.75 K is 46.89 psi. Therefore for the orifice to cavitate at the lip we will have to set the inlet pressure around 80 psi. Similarly, Figure 4 shows the time averaged velocity distribution in the orifice and the pipe along with a line plot for the axial velocity distribution along the centerline of the pipe-orifice configuration. The flow accelerates in the orifice from the freestream velocity of 5.58 m/s to just over 21 m/s.

The instantaneous velocity distribution is depicted in Figure 5 and shows the formation of the jet through the orifice as the flow accelerates to negotiate the area reduction near the throat of the orifice. The velocity distribution also shows shedding from the lip of the orifice. Furthermore, as the jet breaks up and spreads it interacts with the wall and forms a feedback loop which in turn further breaks up the jet. The instantaneous pressure distribution on the symmetry plane is plotted in Figure 6 and shows (i) the formation of a low pressure region near the throat of the orifice as well as (ii) localized pockets of low pressure zones that migrate downstream from the throat. Pressure spectra plots for probes located on the walls in a plane perpendicular to the symmetry plane are shown in Figure 7. The plane located closest to the orifice shows two dominant tones of 150 Hz and 714 Hz. The 150 Hz tone appears to be caused by the flow that comes back towards the orifice after the jet interacts with the wall. The 714 Hz tone appears to be a characteristic of the jet - it represents the time period between two adjacent vortices as they impinge on the wall. The impingement leads to a pressure wave that propagates in the pipe resulting in this frequency being picked up by most of the other probes in the pipe. The three probes in the middle show multiple frequencies being excited indicating a multitude of characteristic scales. At the last probe downstream, closest to the exit, we see a couple of low frequency modes which might be related to the flapping of the jet and the 714 Hz tone that was seen earlier.

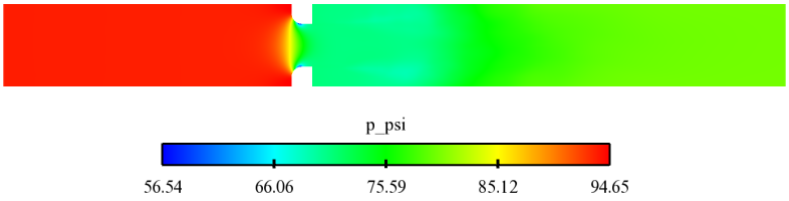

(a) Instantaneous Velocity Distribution

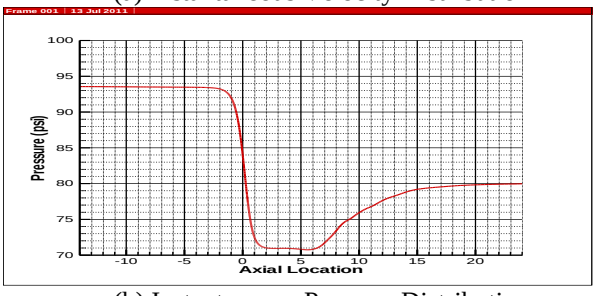

(b) Instantaneous Pressure Distribution

Figure 3. Time-Averaged Pressure Distribution and centerline pressure for simulation of flow through a single hole orifice

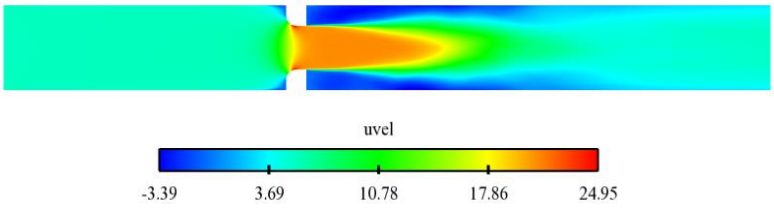

(a) Time-Averaged Velocity Distribution

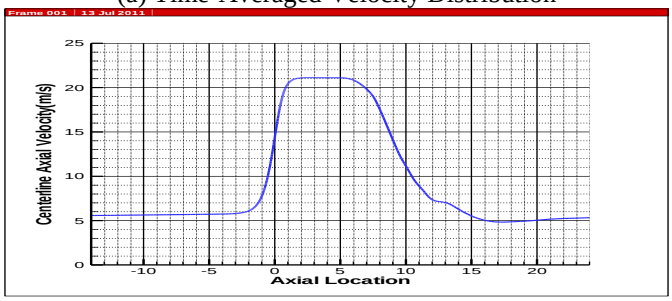

(b) Centerline Velocity Distribution

Figure 4. Time-Averaged Velocity Distribution and centerline velocity for simulation of flow through a single hole orifice

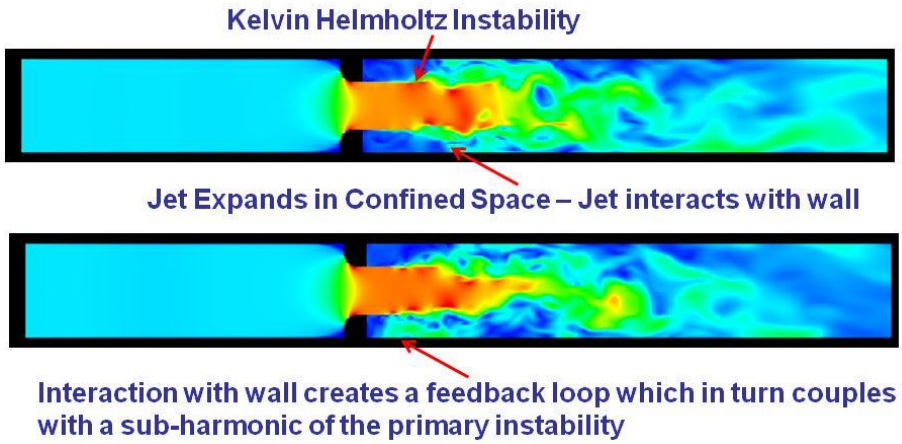

Figure 5. Instantaneous Snapshot of velocity distribution for simulation of flow through a single hole orifice

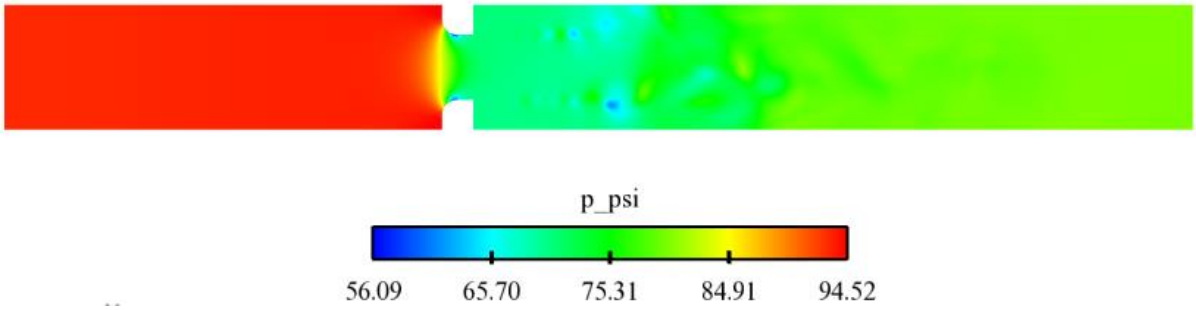

Figure 6. Instantaneous Snapshot of pressure distribution for simulation of flow through a single hole orifice

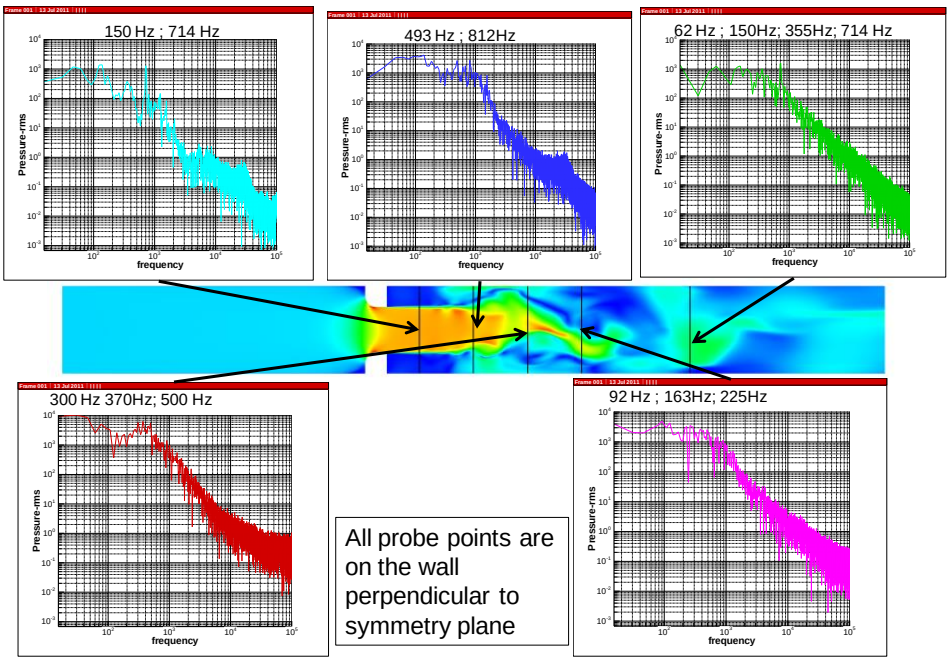

Figure 7. Wall pressure data recorded on probes in a plane perpendicular to the plane of symmetry. The axial location of the probes are shown by the black lines intersecting the plane of symmetry

B. Cavitation Simulations of Single Hole Orifice Element

Cavitation simulations were performed next by lowering the inlet pressure to 80 psi with the unsteady cavitation model detailed in Section IIB. In these simulations the flow is seeded with bubbles that have a radius of 1.2 microns. In this case also, the primary jet from the orifice becomes unstable and starts breaking up approximately a pipe diameter downstream of the vena contracta. Again the instantaneous pressure distribution (Figure 8) shows the shedding of low pressure vortex cores from the lip of the orifice. The shedding phenomena is very periodic and the vortices grow as they convect downstream. However, unlike free jets, the walls confine the growth of the convected vortices. Beyond a certain size, the vortices interact with the wall leading to an increase in pressure at the wall.

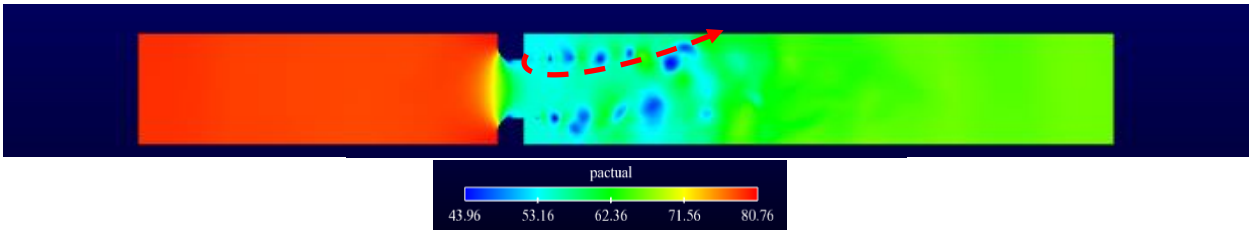

Figure 8. Instantaneous snapshot of pressure for the cavitating simulation

The big difference in the cavitating simulations from the single phase simulations discussed earlier is the formation of a small vapor cavity in the vena contracta of the orifice. This vapor cavity sheds a vapor wake downstream of the orifice (Figure 9). The vapor wake interacts with the vortices that are shed from the lip of the orifice generating large clouds of vapor primarily due to the low pressure associated with the vortex cores. These vapor clouds grow as they convect downstream, in some cases coalescing due to effect of vortex pairing. Ultimately, these vaporous clouds condense either due to the pressure recovery downstream or due to the increase in pressure from their interaction with the wall. The void fraction distribution in Figure 9 shows some very interesting aspects related to the instability mechanisms of the single hole orifice: firstly, not all the vortex cores cavitate or lead to the formation of vaporous clouds indicating that the frequency associated with cavitation instability is lower than the governing fluid dynamic instability. It may or may not be a sub-harmonic of the governing wake-vortex instability; secondly, the cavitation clouds are very asymmetric leading to the conclusion that axisymmetric simulations of these instability mechanisms would be deficient.

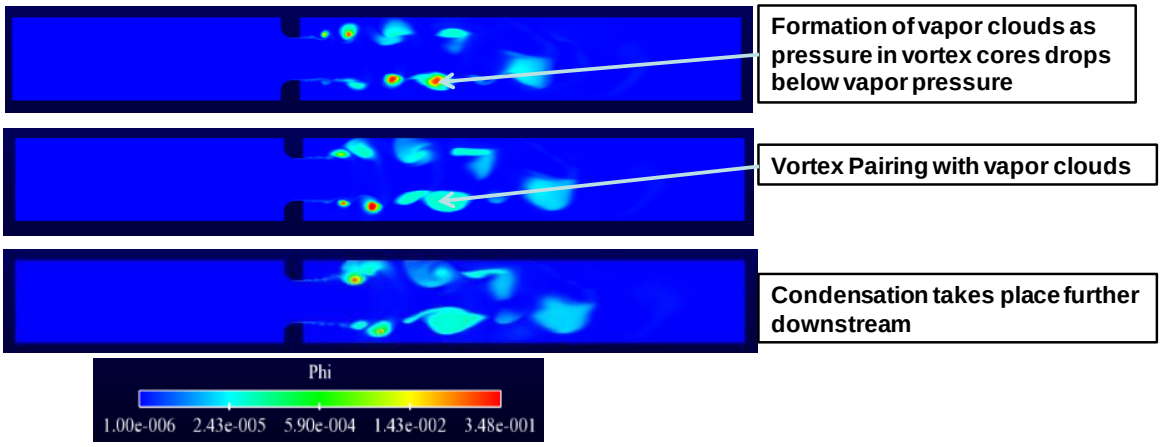

Figure 9. Snapshots of vapor void fraction showing the formation of vapor clouds downstream of the orifice

The pressure recovery downstream in the pipe causes condensation to take place generating large amplitude pressure spikes (Figure 10). The pressure waves propagate downstream in the piping system where they can interact with other components such as valves etc. Pressure spectra of probe points at exact same locations as the single phase case above are shown in Figure 11. The plane closest to the orifice shows its energy distributed among the 386, 641 and 750 Hz. However, the amplitude of the pressure fluctuations is relatively weak compared to the next two probes further downstream. The 386 Hz is approximately half-tone of the frequency related to vapor vortices condensing on the wall. This creates a pressure pulse that travels downstream and is picked up by most of the other probes. The half tone could possibly be related to phase difference between vortices azimuthally or from vortex pairing before their interaction with the wall. The second probe shows distinct tones of 132 Hz, 320 Hz and 386 Hz. The 320 Hz is a sub-harmonic of the 641 Hz that is picked up by the probe closest to the orifice, and the 386 Hz that is common to both the probes is coming from the pressure pulse set up by the cavitation instability. The third probe shows more energy in its tones with a very dominant tone of 330Hz and a sub-harmonic of 165 Hz. It also shows significant energy in a 500 Hz tone that was seen in the single phase simulations for this probe location. The 386 tone is also seen in all the rest of the probes. The pressure spectra in the cavitating simulation is richer than the one seen in the single-phase indicating that the energy is spread across multiple frequencies due to the presence of additional instability mechanisms.

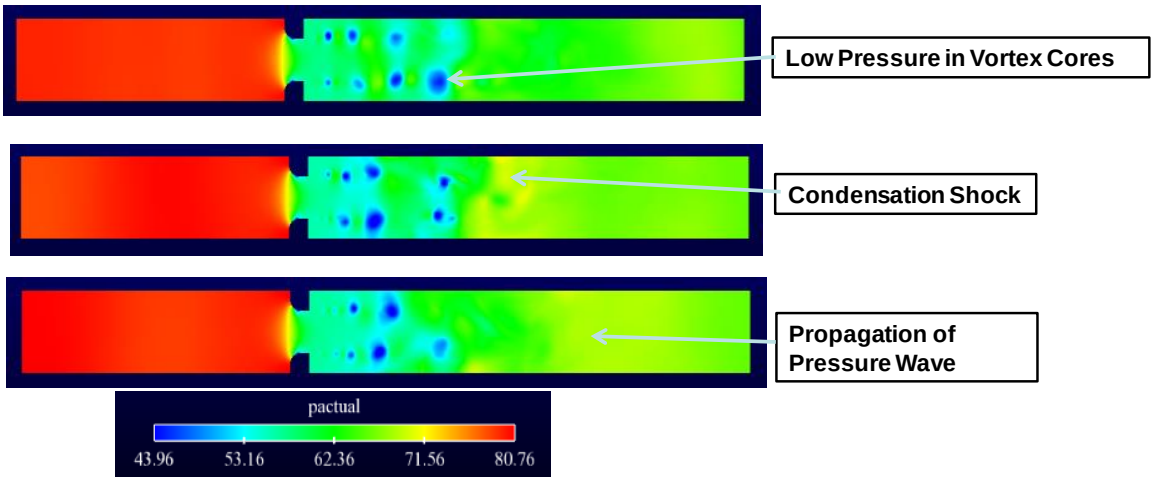

Figure 10. Snapshots of pressure distribution showing the formation of low pressure regions in the convected vortex cores where susceptibility to cavitation is high

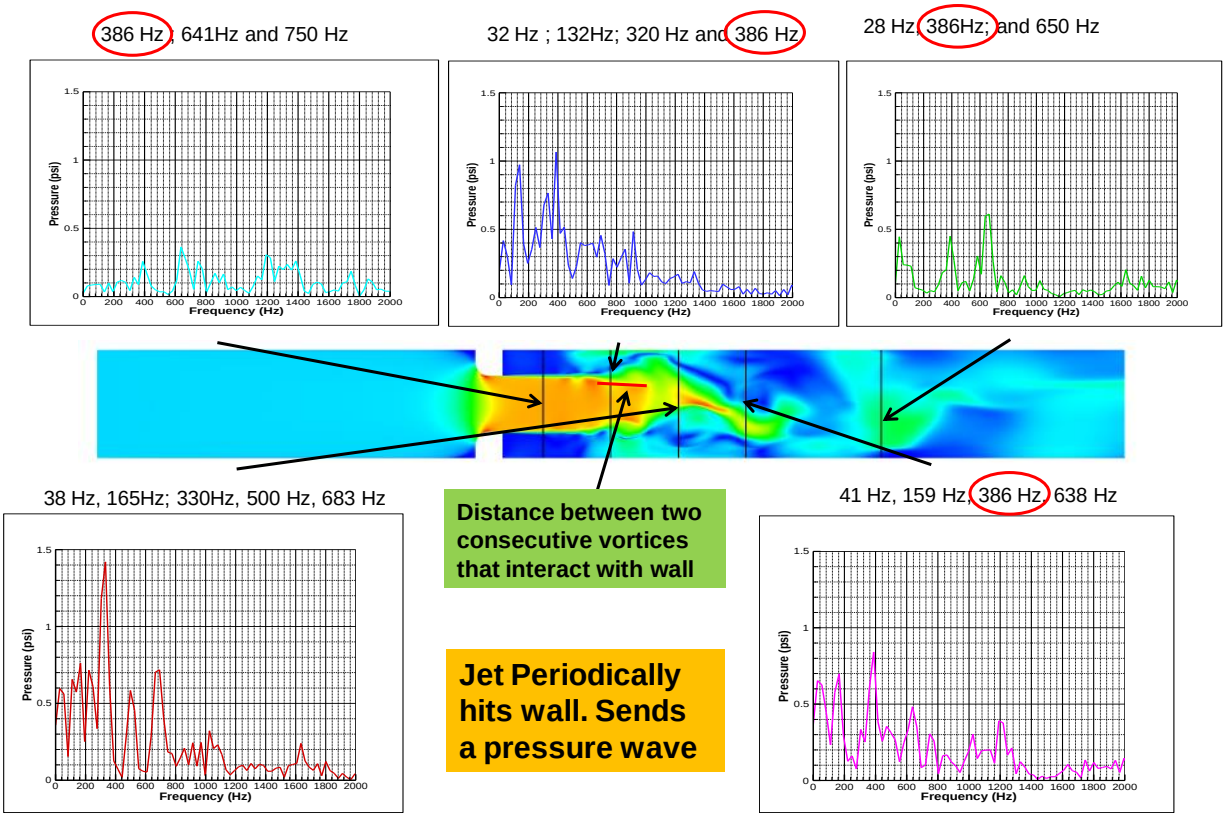

Figure 11. Wall pressure data recorded on probes in a plane perpendicular to the plane of symmetry. Probe locations are identical to single phase simulations. Color of plots is also the same for corresponding location in the single phase spectra plot

IV. Conclusions

A series of high-fidelity three dimensional large eddy simulations (LES) were carried out for a traditional single hole orifice element. The CFD simulations show that the flow through an orifice is highly complex and is characterized by (i) wake-vortex instability (ii) cavitation instability (iii) feedback from re-circulating flow at the step. The primary wake vortex instability is associated with shedding behind the lip of the orifice and has the highest tones although all three instability mechanisms contribute to the rich tonal content that is observed. The cavitation instability is generated because the pressure in the vortex cores falls below the saturation pressure. The cavitation instability is found to have a lower frequency than the primary wake-vortex instability. Furthermore, it was observed that there is considerable asymmetry of the vortex shedding and the cavitation processes as we move away from the lip of the orifice. The asymmetry could be responsible for flapping modes or azimuthal modes although none were observed possibly due to the small run time of the numerical simulation. The interaction of the vortices with the pipe wall is largely responsible for the pressure fluctuations seen in piping systems with an orifice type control element. Probes close to three diameters downstream of the orifice pick up the largest amplitude fluctuations as this location is closest to where the jet spreads out to the wall.

V. Acknowledgments

The work presented in this paper was performed under the NASA STTR program under contract NNX11C143P. The authors would like to thank Dr. Daniel Allgood for his support and technical guidance during the course of the program.

References

[1] Moussou, P., Testud, Ph., Auregan, Y., and Hirschberg, "An Acoustic Criterion for the Whistling of Orifices in Pipes", Proceedings of PVP2007 2007 ASME Pressure Vessels and Piping Division Conference, San Antonio, TX, July 22-26, 2007.

[2] Ahuja, V., and Hosangadi, A., "Analyses of Unsteady Cavitation in Rocket Feed Systems and Flow Control Elements," Paper No. 80, International Symposium on Cavitation, CAV2006, Wageningen, The Netherlands, 11-15 Sept. 2006.

[3] Ahuja, V., Hosangadi, A., Shipman, J., Daines, R. and Woods, J., "Multi-Element Unstructured Analyses of Complex Valve Systems," *Journal of Fluids Engineering*, Vol. 128, No. 4, pp. 707-716, July 2006.

[4] Hosangadi, A., and Ahuja, V., "Numerical Study Of Cavitation In Cryogenic Fluids," *Journal of Fluids Engineering*, Vol. 127, pp. 267-281, March 2005.

[5] Noiray, N., Durox, D., Schuller, T., and Candel, S., "Mode Conversion in Acoustically Modulated Confined Jets", *AIAA Journal*, Vol. 47, No. 9, September 2009.

[6] MacDonald, M.E., Canino, J.V., and Heister, S.D., "Non-linear Response of Plain-Orifice Injectors to Nonacoustic Pressure Oscillations", *Journal of Propulsion and Power*, Vol. 23, No. 6, Nov-Dec 2007.

[7] Lemmon, E.W., Peskin, A.P., McLinden, M.O., and Friend, D.G., (2000) "NIST Thermodynamic and Transport Properties of Pure Fluids", NIST Standard Reference Database 12, Users Guide.

[8] Hosangadi, A., Sinha, N., and Dash, S.M., "A Unified Hyperbolic Interface Capturing Scheme for Gas/Liquid Flows," AIAA-97-2081, 13th AIAA CFD Conferences, Snowmass, CO, June 29-July 2, 1997.

[9] Arunajatesan, S., and Sinha, N., "Hybrid RANS-LES Modeling For Cavity Aeroacoustic Predictions," *International Journal of Aeroacoustics*, Vol. 2, No. 1, pp. 65-73, 2003.